High Cationic Charge and Bilayer Interface-Binding Helices in a Regulatory Lipid Glycosyltransferase[†,‡]

Jesper Lind,[§,⊥] Tuulia Rämö,[§,⊥] Maria L. Rosén Klement,[§] Elsa Bárány-Wallje,[§] Richard M. Epand,[∥] Raquel F. Epand,[∥] Lena Mäler,*[,§] and Åke Wieslander*[,§]

Center for Biomembrane Research, Department of Biochemistry and Biophysics, Stockholm University, SE-10691 Stockholm, Sweden, and Department of Biochemistry and Biomedical Sciences, McMaster University, Hamilton, Ontario, Canada

Received January 10, 2007; Revised Manuscript Received March 18, 2007

ABSTRACT: In the prokaryote *Acholeplasma laidlawii*, membrane bilayer properties are sensed and regulated by two interface glycosyltransferases (GTs), synthesizing major nonbilayer- (alMGS GT) and bilayer-prone glucolipids. These enzymes are of similar structure, as many soluble GTs, but are sensitive to lipid charge and curvature stress properties. Multivariate and bioinformatic sequence analyses show that such interface enzymes, in relation to soluble ones of similar fold, are characterized by high cationic charge, certain distances between small and cationic amino acids, and by amphipathic helices. Varying surface contents of Lys/Arg pairs and Trp indicate different membrane-binding subclasses. A predicted potential (cationic) binding helix from alMGS was structurally verified by solution NMR and CD. The helix conformation was induced by a zwitterionic as well as anionic lipid environment, and the peptide was confined to the bilayer interface. Bilayer affinity of the peptide, analyzed by surface plasmon resonance, was higher than that for soluble membrane-seeking proteins/peptides and rose with anionic lipid content. Interface intercalation was supported by phase equilibria in membrane lipid mixtures, analyzed by ^{31}P NMR and DSC. An analogous, potentially binding helix has a similar location in the structurally determined *Escherichia coli* cell wall precursor GT MurG. These two helices have little sequence conservation in alMGS and MurG homologues but maintain their amphipathic character. The evolutionary modification of the alMGS binding helix and its location close to the acceptor substrate site imply a functional importance in enzyme catalysis, potentially providing a mechanism by which glycolipid synthesis will be sensitive to membrane surface charge and intrinsic curvature strain.

For the function of integral as well as peripheral membrane proteins, several properties of the lipid bilayers must be maintained, for example, (i) a liquid-crystalline state, (ii) a critical thickness (chain length), (iii) a certain surface charge density (potential), given especially by the anionic lipids, and (iv) a fraction of nonbilayer-prone lipids, yielding a curvature elastic stress. The exact mechanisms by which these features are sensed and regulated are unknown in most instances. In *Escherichia coli* plasma (inner) membrane there is a more or less constant composition of zwitterionic and anionic lipid polar (headgroup) species, whereas the liquid state and curvature properties are both regulated at the acyl chain level (*1*) and where temperature is a key factor (*2*). The small, cell wall-less prokaryote *Acholeplasma laidlawii* seems to control both the surface charge density and curvature properties by two consecutively acting, membrane surface-bound lipid glucosyltransferases (*3*), synthesizing two major, nonbilayer-prone and bilayer-forming glucolipids, respectively (*4*, *5*), by adding sugar headgroups to a diacylglycerol acceptor backbone. The strongly varying molar fractions of these, that is, monoglucosyl-diacylglycerol (MGlcDAG[1]) and diglucosyl-diacylglycerol (DGlcDAG), and acylated variants thereof, largely determine the phase equilibria and curvature properties of the *in vivo* lipid bilayer mixture (*6*, *7*). The mechanism seems to respond to several

[†] This work was supported by the Swedish Science Research Council, and the Natural Sciences and Engineering Council of Canada.

[‡] The chemical shifts for 65S-L87 in DHPC (zwitterionic bicelles) and 10% negatively charged bicelles have been deposited with the BMRB (www.bmrb.wisc.edu) under accession code 15171. The coordinates for the solution structure of 65S-L87 in DHPC have been deposited with the PDB under accession code 1Z2T (www.rcsb.org).

* To whom correspondence should be addressed. Tel: +46-8-162448. Fax: +46-8-155597. E-mail: lena.maler@dbb.su.se (L.M.) Tel: +46-8-162463. Fax: +46-8-153679. E-mail: ake.wieslander@dbb.su.se (A.W.).

[§] University of Stockholm.

[∥] McMaster University.

[⊥] These authors contributed equally to this work.

[1] Abbreviations: MGlcDAG, monoglucosyl-diacylglycerol; GT, glycosyltransferase; alMGS, *A. laidlawii* MGlcDAG synthase (lipid GT); PLS-DA, partial least squares analysis-discriminant analysis; ACC, autocross-covariance; DHPC, 1,2-dihexanoyl-*sn*-glycero-3-phosphocholine; DMPC, 1,2-dimyristoyl-*sn*-glycero-3-phosphocholine; DOPC, 1,2-dioleoyl-*sn*-glycero-3-phosphocholine; DOPE, 1,2-dioleoyl-*sn*-glycero-3-phosphoethanolamine; DPoPE, 1,2-dipalmitoleoyl-*sn*-glycero-3-phosphoethanolamine; DMPG, 1,2-dimyristoyl-*sn*-glycero-3-phosphoglycerol; DOPG, 1,2-dioleoyl-*sn*-glycero-3-phosphoglycerol; SDS, sodium dodecyl sulphate; CD, circular dichroism; SPR, surface plasmon resonance; NMR, nuclear magnetic resonance; NOESY, nuclear Overhauser effect spectroscopy; NOEs, proton−proton distances shorter than 6 Å as determined from NOESY cross-peaks; TM, transmembrane; TOCSY, total correlation spectroscopy; RMSD, root mean square deviation; S65-L87, binding helix 65-SLKGFRLVLFVKRYVRKM-RKLKL-87 in alMGS.

10.1021/bi700042x CCC: $37.00
Published on Web 04/20/2007

membrane "packing" stimuli, such as type of acyl chains, various foreign guest molecules, and ionic environment (*8*). The importance of this nonbilayer-prone lipid was recently highlighted by MGlcDAG restoring several malfunctioning protein-mediated membrane processes in a crippled *E. coli* mutant lacking its major nonbilayer-prone lipid phosphatidylethanolamine (PE) by genetic introduction of the MGlcDAG glucosyltransferase (alMGS) yielding large amounts of the "foreign" MGlcDAG (50 mol %) (*9*).

Fold recognition, followed by modeling using two soluble and one membrane-associated glycosyltransferase as templates, yielded similar structure models for both the MGlcDAG and DGlcDAG glucosyltransferases (alMGS and alDGS) (*10*). The two-domain Rossmann folds, of the so-called GT-B type (*11*), both have high isoelectric points especially for the N-domain, which may be important for the established surface binding to anionic phospholipid bilayers (*9*, *10*, *12*). Both enzymes, and related variants in other bacteria, also clearly lack (hydrophobic) transmembrane segments, but detergents are still needed for their solubilization. Analogous features and similar structures apply to the plant galactosyltransferases, synthesizing the major chloroplast galactolipids (Kelly, Wieslander et al., unpublished work). Binding of purified alMGS enzyme to lipid bilayers *in vitro* was stimulated by the presence of anionic phospholipids and also by nonbilayer-prone (neutral) lipids, mainly affecting the association and dissociation phases, respectively, and the kinetics were typical for a two-step process involving a conformational change (*12*). The overall dissociation constant (K_D) was low enough (at least $10^{-10}-10^{-12}$ M), corresponding to an essentially permanent presence of the enzyme on the bilayer surface (interface). Binding to liposomes decreased acyl chain ordering in the bilayer as analyzed by a lipid bis-pyrene probe (*13*), indicating an interface penetration for part(s) of the enzyme. *In vivo*, membrane binding was substantially quenched by increasing intracellular Na^+ or K^+ concentrations (*9*), typical for electrostatic interactions. Together, these data support an association of the alMGS enzyme to the bilayer interphase with electrostatic and hydrophobic interactions, intercalating in between the lipid headgroups, and also involving conformational changes. However, the low activity of the enzyme when bound to a zwitterionic lipid bilayer is strongly stimulated by increased anionic lipids (*12*, *14*), indicating that the enzyme somehow is activated or conformationally modified by such an environment. This may constitute part of the principles for how bilayer properties can control the activity status of these lipid GTs, maintaining correct bilayer packing properties by "feedback loops" to the two synthesizing enzymes. For alMGS *in vitro*, activity is strongly stimulated by increasing amounts of anionic lipids but activity is then retarded at very high amounts (*4*, *14*). Curvature has a modest stimulatory effect on alMGS, whereas the consecutive synthesis of DGlcDAG is strongly affected, in combination with stimulation by anionic lipids (*3*).

Membrane binding regions of alMGS potentially should have some of the features observed for the full size enzyme (cf. above). In general, protein segments interacting with lipid bilayer interfaces reveal essentially no consensus sequence features (*15*, *16*), but amphipathic helices enriched in cationic amino acids are common surface anchors in many proteins, yielding more or less strong associations. For interactions with specific target lipids in bilayers, more or less hydrophobic loops extending from helices or β-strands are frequently involved. By extensive bioinformatic and multivariate approaches, we show here that membrane-bound glycosyltransferases (GT-B fold without TM segments) generally have high pI values for the N-domain and certain property relationships along the aa-sequence, including potential amphipathic helices. A potential helix segment from the alMGS lipid glycosyltransferase was selected, corresponding to a proposed membrane-binding segment in the established structure of the *E. coli* cell-wall-precursor glycosyltransferase MurG (*17*) and parts of the substrate-binding region in structurally related but soluble glycosyltransferases such as Gtf-A, -B, and -D (*18*−*20*). With several methods for structural and binding analyses, it is shown to have conformational and lipid-binding features strongly dependent on the surrounding lipid matrix.

EXPERIMENTAL PROCEDURES

Bioinformatic Methods. Sequences related to the *A. laidlawii* MGlcDAG synthase (lipid glucosyltransferase alMGS) (*21*) were searched by PSI-BLAST at NCBI (www.ncbi.nlm.nih.gov/BLAST/). Selected hits with experimentally established functions, and/or at least ≈27% identical aa sequences (e-30), were aligned with ClustalW (www.ebi.ac.uk/services/). Prediction of secondary structure and fold recognition were done by 3D-Jury using many methods from the MetaServer (http://bioinfo.pl/meta/). Conservation and variation of aa residues in the obtained alMGS 3D-structure model, in relation to the related enzymes retrieved by BLAST, were analyzed at the ConSurf server (http://consurf.tau.ac.il/). Potential transmembrane segments in the proteins were searched by TMHMM (www.cbs.dtu.dk/services/), and potential bilayer interfacial segments (*22*) were analyzed by Membrane Protein Explorer (Jaysinghe, S., Hristova, K., Wimley, W., Snider, C., and White, S. H. (2006); http://blanco.biomol.uci.edu/mpex). Hydrophobic moment ("amphipathicity") was analyzed at http://www.doe-mbi.ucla.edu/. Amino acid residues potentially involved in substrate binding were analyzed at the SEARCH GTr database (for GTs in natural product biosynthesis) (http://linux1.nii.res.in/~pankaj/gt/gt_DB/html_files/searchgtr.html).

Multivariate Sequence Analysis. Periodic physical features in the GT protein sequences that may identify them according to localization, that is, soluble or membrane-bound, were analyzed by multivariate methods. Amino acid properties can be described and characterized in many ways. To decrease the number of parameters that describes *each* amino acid, so-called *z-scales* were used here. These are derived from 29 physical−chemical experimental parameters with principal component analyses (*23*) and can approximately be translated as $\mathbf{z_1}$ *hydrophobicity/hydrophilicity*, $\mathbf{z_2}$ *bulk of sidechain*, and $\mathbf{z_3}$ *polarizability/charge*. Property periodicities in the GTs were described by *auto-cross-covariance* (ACC) in the *z*-values, yielding many interaction terms within long sliding windows ("lags") (cf. Figure 1 in ref *24*). For large polypeptides such as the glycosyltransferases here, the optimal lag seems to be between 15 and 25 aa (data not shown).

This is followed by *partial least-squares projections to latent structures discriminant analysis* (PLS-DA), which

Table 1: Soluble and Membrane-Bound Glycosyltransferases[a]

organism	function	calculated pI full/N-/C-domain[c]	UniProt identifier
	membrane		
Acholeplasma laidlawii	MGlcDAG synthase	9.5/9.8/5.5	Q93P60_ACHLA
Acholeplasma laidlawii	DGlcDAG synthase	9.4/10.0/6.4	Q8KQL6_ACHLA
Arabidopsis thaliana	DGalDAG synthase 1	7.6/8.4/6.8	Q9S7D1_ARATH
Arabidopsis thaliana	DGalDAG synthase 2	8.7/8.8/6.4	O65264_ARATH
Arabidopsis thaliana	MGalDAG synthase C	8.5/8.8/6.6	Q9SI93_ARATH
Arabidopsis thaliana	sterol GT	6.3/7.2/5.4	O23649_ARATH
Arabidopsis thaliana	sulfolipid synthase	8.6/9.8/4.8	Q8S4F6_ARATH
Arabidopsis thaliana	SQDAG synthase	7.1/9.4/4.7	Q9LFB4_ARATH
Avena sativa	sterol GT	5.8/6.1/5.2	O22678_AVESA
Bacillus subtilis	processive lipid GT YpfP	8.5/9.3/5.6	YPFP_BACSU
Borrelia burgdorferi	MGalDAG synthase	9.7/10.0/8.8	O51410_BORBU
Cucumis sativus	MGalDAG synthase A	9.2/9.5/8.2	P93115_CUCSA
Escherichia coli	cell-wall GT MurG[b]	9.7/10.8/5.9	MURG_ECOLI
Escherichia coli	Lps heptosyltransferase[b,d]	7.2/9.7/5.6	RFAF_ECOLI
Neissera meningiditis	cell-wall GT MurG	8.8/9.9/5.5	MURG_NEIMA
Pseudomonas aeruginosa	rhamnosyltransferase	8.8/8.9/8.0	Q51560_PSEAE
Pseudomonas paucimobilis	glucoronosyltransferase GelK	8.7/10.0/5.2	Q9APE1_PSEPA
Staphylococcus aureus	processive lipid GT YpfP	8.9/9.0/7.9	O86492_STAAU
Streptococcus pneumoniae	MGlcDAG synthase	6.1/9.1/4.6	Q97QX1_STRPN
Streptococcus pneumoniae	GalGlcDAG synthase CpoA	6.7/9.3/5.2	O06452_STRPN
	soluble		
Agrobacterium tumefaciens	glycogen synthase 1	6.0/5.3/8.7	GLGA1_AGRT5
Amycolatopsis orientalis	vancomycin GT GtfA[b]	4.8/4.7/5.1	P96558_AMYOR
Amycolatopsis orientalis	vancomycin GT GtfD[b]	5.0/4.7/5.9	Q9AFC7_AMYOR
Arabidopsis thaliana	trehalose phosphate synthase	6.7/6.5/7.8	P93653_ARATH
Aspergillus niger	trehalose phosphate synthase	5.4/5.0/6.3	TPSA_ASPNG
Bacillus subtilis	glycogen synthase	5.3/5.3/5.3	GLGA_BACSU
Bacteriophage T4	DNA β-GT[b]	9.1/9.3/7.1	GSTB_BPT4
Candida albicans	trehalose phosphate synthase	6.3/6.3/6.4	Q9HEP0_CANAL
Escherichia coli	epimerase[b]	5.9/6.1/5.8	WECB_ECOLI
Escherichia coli	glycogen synthase	6.1/6.4/5.4	GLGA_ECO57
Escherichia coli	maltodextrin phosphorylase[b]	7.3/6.4/8.5	PHSM_ECOLI
Escherichia coli	trehalose phosphate synthase[b]	6.4/5.8/8.8	OTSA_ECOLI

[a] GTs of GT-B fold with established localization and function, several determined 3D structures, and from various CAZy families are included. The membrane group contains no transmembrane segments according to predictions and structures. [b] Established 3D-structure. [c] Only two digits shown for pI. C-terminal sequence tail included in N-domain according to structures and fold recognition (cf. Figures 2 and 4). [d] Localization predicted here.

finds the relationships between the X-matrix (periodic sequence properties) and the Y-matrix (group membership), also involving *cross-validation* (*24*). PLS-DA was used with the assumption that sequences belonging to the same localization class have common features and therefore will behave similarly in the analysis, as visualized in the *score plot*. This method can also be used to *predict* class-belongings for unclassified sequences. The PLS model contains information both regarding the relationship among the objects (*scores*) and the contribution of the variables to the model (*PLS weights*). The objects best separated, hence localized far away from the center of the plot, are the ones best described by the variables with the largest weight. Such variables are therefore most likely to be identified at the sequence level in these proteins. A Q^2(cum) value is calculated, which describes how much of the variance in the Y matrix can be predicted by the model. To obtain a perfect score of 1, all objects should be predicted back to the exact position given by the Y matrix. A Q^2(cum) larger than 0.1 corresponds to a 95% significance of the model.

Glycosyltransferase Reference Sequences. For the multivariate analyses, a set of GTs with GT-B fold and experimental verification of membrane (or lipid bilayer) localization, plus a set of soluble ones were selected (Table 1). Here, a distribution from various CAZy GT-families and ones with established 3D-structures as well as avoiding bias from enzymes with too similar aa-sequences, was important. The isoelectric points for full size GTs and their N- and C-domains (according to the MetaServer) were calculated. Several *in silico* mutants of these, with swapped helical segments and N/C domains, were also constructed and included in the calculations.

Materials. The peptide corresponding to the potential alMGS membrane-binding segment (65-SLKGFRLVLF-VKRYVRKMRKLKL-87) was synthesized and purified (immunograde) by NeoMPS SA, France. The lipids 1,2-dimyristoyl-*sn*-glycero-3-phosphocholine (DMPC), 1,2-dihexanoyl-*sn*-glycero-3-phosphocholine (DHPC), and 1-palmityl-2-steroyl-(5-DOXYL)-*sn*-glycero-3-phosphocholine as well as chain-deuterated DHPC-d_{22} and DMPC-d_{54} were all purchased from Avanti Polar Lipids, USA, and 1,2-dimyristoyl-*sn*-glycero-3-[phospho-rac-(1-glycerol)] (DMPG) and chain-deuterated DMPG-d_{54} were from Larodan AB, Sweden.

Bicelle Preparation. Bicelles were produced by vortexing the long-chain lipid DMPC together with the peptide in H_2O. DHPC dissolved in H_2O was then added and vortexed, rendering a sample with 1 mM peptide, 50 mM DMPC, and 200 mM DHPC. The size of the bicelles can be roughly estimated by the ratio q = [long chained lipid]/[short chained lipid], and in these experiments, bicelles with $q = 0.25$ were used. Acidic bicelles were prepared by exchanging 10% or

30% of DMPC for DMPG. In the bicelle experiments, the pH was adjusted to 5.7 with a 100 mM phosphate buffer. In all samples, 10% of D_2O was added for field/frequency lock stabilization during the NMR experiments. The samples containing peptide together with DHPC were prepared by mixing 1 mM peptide with 100 mM of DHPC.

CD Spectroscopy. All CD spectra were recorded in the wavelength range between 190 and 250 nm on a JASCO J-720 CD spectropolarimeter using a bandwidth of 0.2 nm. A quartz cuvette with a path length of 0.05 mm was used, requiring approximately 150 μL per sample. The spectra were recorded at 37 °C with 10 scans each. The α-helix content was estimated by measuring the mean residue ellipticity at 222 nm. From assuming a two-state equilibrium between α-helix and random coil conformation, the percentage of α-helical conformation can be estimated (*25*).

Preparation of Liposomes. Lipids in chloroform solutions were mixed to contain DOPC from 100 mol % to 60 mol % and DOPG from 0 mol % to 40 mol %. The solvent was removed under N_2-flow overnight. Dried lipids were resuspended to 10 mM in 1 mL of 10 mM HEPES at pH 7.4, 150 mM NaCl, and 0.1% DMSO. Hydration of lipid films was done at room temperature by extensive vortexing. Lipid solutions were then pushed through double polycarbonate filters, 0.1 μm pore size, 21 times using a 1-mL extruder (Avestin LiposoFast) to yield unilamellar vesicles (*26*). Liposomes were stored at +8 °C.

Binding Analysis with Surface Plasmon Resonance. SPR was carried out on a BIAcore 3000 instrument (Biacore AB, Sweden) using Sensor Chip L1 and 10 mM Hepes at pH 7.4, 150 mM NaCl, and 0.1% DMSO as running buffer. The chip surface was cleaned with 40 mM *n*-octyl-β-glycoside (20 μL, 20 μL/min) and running buffer (50 μL, 20 μL/min). Liposomes with varying lipid composition were injected (30 μL, 3 μL/min) giving a response of 2000−4500 response units (RU). Ten millimolar NaOH (50 μL, 50 μL/min) was injected to remove multilamellar vesicles. The resulting membrane surface was then coated with 3 mM DOPC liposomes (10 μL, 2 μL/min) to obtain a similar level, 4000−7000 RU, of liposome immobilization. Removal of multilamellar vesicles was repeated by injecting 10 mM NaOH (50 μL, 50 μL/min). Injection of running buffer (50 μL, 5 μL/min) was done to obtain a stable baseline. Peptide was injected (25 μL, 5 μL/min) using the KINJECT command; both association and dissociation were followed for 5 min. Regeneration was done by double injection of 50% 2-propanol in 50 mM NaOH (10 μL, 5 μL/min).

Solution NMR Spectroscopy. All ^{1}H NMR spectra were recorded on a Varian Inova NMR spectrometer operating at a ^{1}H frequency of 600 MHz at 37 °C. NOESY spectra (*27*) and TOCSY spectra (*28*) were recorded in order to calculate the secondary and tertiary structure of the alMGS peptide in membrane mimetic environments. The NOESY spectra were recorded with a mixing time of 100 ms, while the TOCSY spectra were recorded with 20, 30, and 80 ms; 2048 data points were collected in the t_2-dimension and 512 data points in the t_1-dimension. The water signal was suppressed with the WATERGATE method (*29*). The spectra were processed with FELIX (Accelrys, version 2001.1), and the processing included zero-filling to 4096 × 2048 data points prior to Fourier transformation.

Structure Calculation. Resonance assignments for S65-L87 in DHPC, zwitterionic bicelles, and in 10% acidic bicelles were obtained using a combination of the TOCSY spectra and sequential NOESY cross-peaks. A solution structure of the peptide in 100 mM DHPC was calculated on the basis of NOESY-derived distance constraints. The NOESY cross-peaks were categorized into three different groups depending on intensity. These groups were classified as strong, medium, and weak intensities and were assigned the upper distance limits <3.5 Å, < 4.5 Å, and <6 Å. In total, 188 upper distance constraints were used to calculate structures. The upper limits were adjusted iteratively during structure calculation. Fifty structures were calculated using the program DYANA (version 1.5) (*30*), and the 24 best structures, as judged from violation energies and DYANA target function, were selected. The quality of the final ensemble of structures was evaluated by examining Ramachandran maps, bond geometry, and secondary structure by using the program PROCHECK-NMR (*31*).

Positioning Studies. 1-Palmityl-2-steroyl-(5-DOXYL)-*sn*-glycero-3-phosphocholine was dissolved in methanol and added to the S65-L87 peptide dissolved in neutral bicelle solution and to the peptide dissolved in 10% acidic bicelle solution (to a concentration of 0.75 mM 5-DOXYL-labeled lipid in a sample with 1 mM peptide and 250 mM total lipid). This procedure has previously been demonstrated to be useful in both micellar systems (*32*) and in bicelles (*33*, *34*). The spin-labeled phospholipids have been used to investigate membrane penetration depths in bilayers (*35*, *36*), and at the low molar fractions used here, no bilayer perturbation has been observed. Two-dimensional TOCSY spectra (τ_{mix} = 30 ms) were recorded before and after the addition of the spin-labeled lipid, and by measuring peak intensity reduction in the H^N-H^α fingerprint region, the positions of the residues in the peptide relative to the spin-label were estimated.

^{31}P NMR. The ^{31}P NMR spectra were measured using suspensions containing 25 mg of DOPE/DOPG 7:3 (mol/mol). Films were made from a solution of lipid in chloroform/methanol (2:1, v/v) with or without the addition of a methanolic solution of the S65-L87 peptide to attain the desired lipid-to-peptide ratio. The lipids and peptide were deposited as a film by evaporation of the solvent with nitrogen and then hydrated by vortexing with 200 μL of 20 mM PIPES, 1 mM EDTA, and 150 mM NaCl with 0.002% NaN_3 at pH 7.40. The suspension was then frozen and thawed three times to ensure equilibration and then loaded onto a 5-mm Shigemi NMR tube.

Spectra were obtained using a Bruker DRX-500 spectrometer operating at 202.45 MHz in a 5 mm broad band probe over a 48.6 kHz sweep width in 16 × 1024 data points. A 90° pulse width of 9.4 μs was used. Composite pulse decoupling was used to remove any proton coupling. Spectra were referenced to phosphoric acid assigned a chemical shift of 0 ppm. Generally, 800 free induction decays were processed using an exponential line broadening of 100 Hz prior to Fourier transformation. Probe temperature was maintained to +/−0.2 °C by a Bruker BVT 3000 variable temperature unit. Temperatures were monitored with a calibrated thermocouple probe placed in the cavity of the NMR magnet.

Differential Scanning Calorimetry (DSC). Each sample contained 10 mg of DPoPE in chloroform/methanol (2:1,

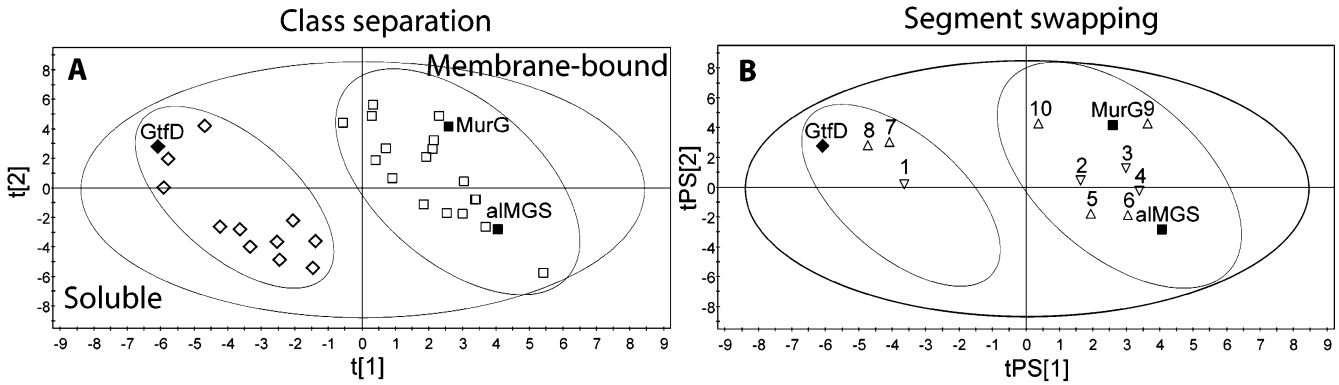

FIGURE 1: Separation of membrane-bound and soluble glycosyltransferases on basis of sequence property patterns. (A) Score plot from the multivariate PLS-DA analysis of all ACC terms (combinations of *z* variables) within a sliding window of 19 aa (*24*). The membrane-bound enzymes form a clear cluster, with three significant PLS components separating the groups and a $Q(\text{cum})^2$ value for the model of 0.52 ("predictability", cf. Experimental Procedures). The two first components (score vectors t1 and t2) are shown. The sequence sets are shown in Table 1. (B) Domain and helix swapping. N- and C-domains, and the aa 65−87 helix in alMGS (and counterparts in GtfD and MurG), were exchanged *in silico* and the hybrids predicted against the model of Figure 1A. (Only the hybrid constructs are shown.) Score vectors tPS1 and tPS2 are for the prediction set (PS). Symbols: 1, N-GtfD/C-alMGS; 2, N-alMGS/C-GtfD; 3, N-MurG/C-alMGS; 4, N-alMGS/C-MurG; 5, alMGS/helix-GtfD; 6, alMGS/helix-MurG; 7, GtfD/helix-alMGS; 8, GtfD/helix-MurG; 9, MurG/helix-alMGS; and 10, MurG/helix-GtfD.

v/v), and to some, a small aliquot of a methanolic solution of the S65-L87 peptide solution was also added. The mixtures were then made into a film by solvent evaporation and processed essentially as described above for the ^{31}P NMR samples. The lipid suspension was vortexed extensively and degassed under vacuum before being loaded into a NanoCal high sensitivity scanning calorimeter (CSC, Lindon, UT). A heating scan rate of 0.75°/min was employed. The bilayer to hexagonal phase transition was fitted using a deconvolution program provided by MicroCal Inc. (Northampon, MA) with parameters to describe equilibrium with a single van't Hoff enthalpy and the transition temperature reported as that for the fitted curve.

RESULTS

Sequence and Structure versus Membrane Localization. Glycosyltransferases (GT) are among the largest groups of proteins; currently, the many thousand genes/proteins (ORFs) are divided into 89 families on the basis of aa similarities (http://www.cazy.org/CAZY/fam/acc_GT.html). However, only a limited number of structures have been determined so far, essentially just two main structural fold groups (*11*) with only one example of an established membrane-associated GT, the *E. coli* cell wall precursor GT MurG (*17*). According to fold recognition analyses (at the MetaServer, cf. Experimental Procedures), the alMGS glucosyltransferase is predicted to have a structure similar to those of several soluble glycosyltransferases (with high scores), such as glycogen synthase and the vancomycin GT GtfB (pdb codes 1rzu and 1iir, respectively) of the GT-B fold type with two Rossmann-like domains (data not shown). All of the selected membrane and soluble GTs (Table 1) contain several short sequence segments with favorable ΔG for an interfacial (hydrophobic) lipid bilayer binding, according to predictions at the Membrane Protein Explorer (http://blanco.biomol.uci.edu/), but no transmembrane segments according to TMHMM (data not shown). Especially, single transmembrane segments are common for lipid glycosyltransferases in, for example, the endoplasmic reticulum. Some of the predicted interfacial segments predicted here were confined to the core β-strands in the established structures and are not likely to contribute any properties to the protein surfaces or membrane binding. Hence, it was evident from these analyses that established hydrophobicity sequence analyses fail to clearly discriminate this group of surface-associated membrane enzymes from soluble ones. However, the calculated isoelectric points for especially the N-domain of the membrane GTs seem to be substantially higher than those for the soluble ones, which should yield a strongly plus-charged character at physiological pH (Table 1).

Discrimination by Multivariate Sequence Property Analyses. Glycosyltransferases of the GT-B fold attaching the donor sugar substrate in α or β configuration can be discriminated from each other by multivariate analysis of their sequence property patterns by PLS-DA (partial least-squares projections to latent structures discriminant analysis) (*24*). An analogous separation of the membrane and soluble GT-B fold ones was achieved here; see Figure 1A. This PLS score plot reveals two well separated clusters, and the model has 3 significant PLS components and a $Q^2(\text{cum})$ value for the model of 0.52 (high predictability; cf. Experimental Procedures). One protein, the *E. coli* heptosyltransferase (Table 1) with a recently established 3D-structure (pdb code 1psw) was predicted here to belong to the membrane-bound group (data not shown).

For essentially all GT-B fold GT structures determined, the β-sheet cores of the Rossmann-like domains are the most similar, especially the C-domains, and differences between structures are more pronounced at the helices and loops of the protein surfaces (*11*, *37*). An analysis of the PLS weights behind the sequence differences between the membrane and soluble groups (data not shown) were retrieved from the major property periodicity (*auto-cross-covariance*; ACC) variables important for the separation of the membrane group in Figure 1A. The top ones were (in rank) pI of N-domain, pI of full enzyme, $z_2 1 * z_3 9$, $z_3 1 * z_3 9$, $z_3 1 * z_1 3$, and $z_3 1 * z_3 3$ (being larger for the membrane group), and where the two first variables were substantially stronger than all the following ones. z_1 is *hydrophobicity/hydrophilicity*, z_2 *bulk of side chain* (volume), and z_3 is *polarizability/charge* (see

Red color, α-helix; and blue, β-strand in template structures (predicted for alMGS)

FIGURE 2: Comparison of alMGS glucosyltransferase with template structure sequences. Alignment and labels of the sequences are from the 3D-Jury fold recognition analyses of alMGS at the MetaServer. Blue, *β*-strand, and red, α-helix, in the structures of MurG and GtfB, and predicted for alMGS (by MetaServer). Black letters in MurG and GtfB indicate (few) deleted positions (by MetaServer) to fit with the alMGS sequence. Underlined sequences show segments likely to associate with a phosphatidylcholine lipid interface according to MPEx analyses (*42*). Gray boxes in alMGS are predicted helical amphilic segments S65-L85 and Y127-L132, with a hydrophobic moment (*42*) larger than 0.50. Yellow box in MurG is the potential membrane-binding segment (helix N3), according to structure determination (*17*). Green boxes in GtfB indicate the hypervariable (substrate-binding) sequence regions (in glycosyltransferase GtfB, GtfD, and GtfA structures) partially overlapping helices N3 and N5 (*18*−*20*). The N/C-domain linker region is marked for GtfB. The aa region 55 to 85 in alMGS, (and the corresponding one in MurG) is strongly enriched in positively charged amino acids, and lacks negative ones.

Experimental Procedures). Hence, ACC variable $z_2$1*$z_3$9 is translated as a recurrent correlation between side-chain volume at sequence position 1 with polarizability/charge at position 9. Of the top 11 ACC variables, 8 dealt with correlations between positions 1*6 to 1*19, whereas only three were from short distances, that is, 1*2 and 1*3 positions (data not shown). From an analysis of the aa-sequences of the determined 3D structures, $z_2$1*$z_3$9 and $z_3$1*$z_3$9 seem to be connected to the distribution (positioning) of aa properties in loops (small hydrophobic) versus position 9 downstream (often a plus-charged aa), frequently in another loop or a helix (data not shown). The $z_3$1*$z_1$3 and $z_3$1*$z_3$3 ACC variables correlated to properties on opposite sides of helices, here in a typical amphipathic organization. $z_3$1*$z_1$3 is read as z_3 (*polarizability/charge*) at position 1 correlating with z_1 (*hydrophobicity/hydrophilicity*) at position 3, that is, on the other side of a helix. These features also include the magnitudes ("property strength") of these *z* variables. Likewise, the $z_3$1*$z_3$3 term deals with different charge (polarizability) properties on the opposite side of helices. This is analogous to the weak amphipathic character (property periodicity) recorded for many helices in soluble proteins (*38*) but is stronger here for the membrane GT group. It is also noticeable that the strong position 1*5 correlation occurring for several aa-patterns and the position 1*5*9 aromatic and glycine motifs in interacting transmembrane helices, that is, all on the same helix face (see (*39*−*41*)), were absent here (data not shown).

By swapping N- and C-domains *in silico* and then predicting the class-belonging for the hybrids in the multivariate model, it was obvious that the N-domain had a large impact for the localization grouping but that the sequence features of the C-domains were different for the membrane and soluble GTs; see Figure 1B. These findings support the presence of highly cationic N-domains, unique sequence−position (property) correlations, and amphipathic helices as important characteristic features of the membrane-bound group of GTs.

Identification of Amphipathic Helices. Two strongly cationic, amphipathic helices with high hydrophobic moment, above the threshold for interface association (*42*), seem to be present in the alMGS N-domain (Figure 2, gray segments). The first is at a sequence position homologous to the suggested membrane-binding region (amphipathic helix) in the MurG structure (Figure 2, yellow segment). Both of these segments and the MurG one were indicated by multivariate analyses (data not shown). These positions are analogous to two of the (sequence) hypervariable substrate binding regions (Figure 2, green segments) of the vancomycin-modifying soluble GTs (*19*). Sugar-DAG lipid GTs closely related to alMGS, selected by BLAST analysis (data not shown), all have a predicted amphipathic helix at a position corresponding to the first alMGS, but sequence conservation is much less for this segment than for the rest of the alMGS-related enzymes, according to analyses at the ConSurf server (cf. Figure 3). However, note the conserved His motif just downstream of the amphipathic segment. Likewise, sequence conservation for the analogous amphipathic segment in MurG (Figure 2, yellow segment; Figure 3, last row) is low in many MurG homologues, as revealed from a BLAST comparison (data not shown). This may indicate that these segments are not only involved in binding the acceptor (lipid) substrates, which are essentially identical within each of the two sets of MGS and MurG enzymes analyzed, respectively. However, the two helices in alMGS and MurG occupy similar positions in the highly plus-charged N-domains, as is evident from Figure 4, indicating similar orientation/positioning of the enzymes with respect to the membrane surface. *In silico* swapping, followed by prediction against the multivariate model (in Figure 1A), showed that these segments were important for class assignment but slightly less so than the full N- or C-domains; see

Species	E-value[§]	Identical aa's (%)[§]	Potential membrane-binding segment[#]	UniProt Accession
*Acholeplasma laidlawii**	0.0	100	59 WVIPRKSLKGFRLVLFVKRYVRKMRKLKLDVVHIHTE 95	Q93P60_ACHLA
Onion yellows phytoplasma	2e-79	40	MPLPFKIFKDYRWVLSYKKHLFKIKALNLDVIHVHTE	Q6YRK6_ONYPE
Treponema denticola	8e-64	36	IPFFKWSEFRIGLFLKHTKAYNKVKALNFDIVHTQTE	Q73L31_TREDE
Listeria monocytogenes	8e-59	32	IPFVFFPERRV-AIAGMNKFIKLVGRLDLDIIHTHTE	Q4EFH0_LISMO
Streptococcus pyogenes	4e-54	34	VPFVSFTDRRV-VYRGLISSYKIAKHYNLDIIHTQTE	Q48US8_STRPM
Enterococcus faecalis	1e-53	33	VPFVSFKDRRV-VVRGMWYAYLIAKELELDLIHTHTE	Q830A6_ENTFA
Streptococcus mutans	2e-51	32	VPFFAFKDRRV-AYAGFTDALKIASRYKLDIIHTHTE	Q301X1_STRSU
Lactobacillus plantarum	2e-50	31	IPFVSFTDRRI-AVRGLFKAYQVAKDLGLDIVHTQTE	Q88XD7_LACPL
*Streptococcus pneumoniae**	5e-49	31	IPFVSFTDRRI-AFRGLFEATKVAKEVNLDIVHTQTE	Q5FLU0_LACAC
Lactococcus lactis	5e-48	32	IPFVSLAERKI-VLKGVFAAYLIAKEYDLDIIHTQTE	Q9CDS5_LACLA
Clostridium acetobutylicum	3e-46	30	FAIGIYPDARI-MKPIKNKIVGEIIKWRPDIIHSQTE	Q97G35_CLOAB
*Borrelia burgdorferi**	1e-44	29	IQINKKLDAVI-AFPNKRKISKIIQSYKPDIIHTHSE	O51410_BORBU
*Thermotoga maritima**	1e-38	29	IPFPFEPQHRI-SIASTKNILEFMRENNVQIIHSHSP	Q9WZK3_THEMA
*Deinococcus radiodurans**	6e-29	27	VRYPLLPTYRL-AWPGR----RSFEQR-YDLIHTHTP	Q9RV05_DEIRA
Escherichia coli MurG (PDB-1FOK)			61 IRISGLRGKGIKALIAAPLRIFNAWRQARAIMKAYKPD 98	MURG_ECOLI

[§]For full length proteins. [#]Black, hydrophobic; green, polar; blue, positive; and red, negative amino acid residues, repectively. *Established enzyme function.

FIGURE 3: Similarities to other lipid glycosyltransferases. alMGS was used as a query in a PSI-BLAST search. The amphipathic segment is the least conserved region sequence-wise, according to analyses at the ConSurf server (http://consurf.tau.ac.il/). Only selected sequences with high similarities are shown, and subspecies variants are omitted. All species contain a monoglycosyldiacylglycerol lipid (except *E. coli*), and in *-labeled ones, the corresponding lipid glycosyltransferase gene has been functionally verified. All proteins (enzymes) belong to GT family 4 of glycosyltransferases in the CAZy database (http://afmb.cnrs-mrs.fr/CAZY/GT.html), except for MurG (GT-28). Sequence segments are aligned by ClustalW of full-length proteins. The alMGS predicted amphiphilic helix and MurG helix Nα3 are underlined; the double lines for MurG indicate exposed aa's of the proposed membrane-binding patch (*17*). MurG sequence similarity to alMGS is below the statistical similarity threshhold (data not shown). Symbols: black, hydrophobic; green, polar; blue, positive; and red, negative amino acid residues.

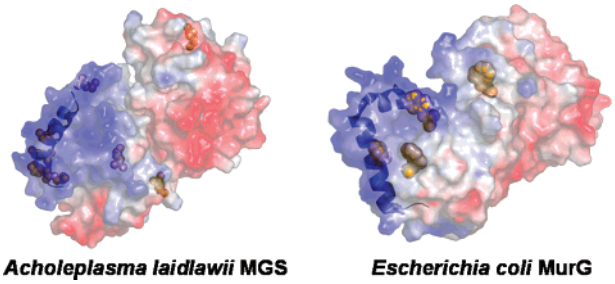

FIGURE 4: Amphipathic helices and surface charge in alMGS and MurG. Visualization of the potential membrane-binding helices in the highly plus-charged N-domains of the alMGS model (*10*) and MurG pdb 1F0K structure (bottom, binding surfaces shown). Blue, cationic; red, anionic; and gray, hydrophobic (cf. aa sequences in Figure 2). The MurG helix was suggested as a potential binding one in the structure analysis (*17*). In alMGS, the eight positively charged residue pairs are marked in yellow (not to scale). The last two pairs (K393−K394 and K397−K398) are not part of the stucture model but lie close to the binding peptide S65-L85 C-end. Such pairs are essentially absent in MurG (only one), which instead contains a number of W residues (yellow label for W85, W116, W137, and W291) in a predicted interface-associating patch including the helix. In alMGS, a conserved EX_7E motif for the donor sugar nucleotide is localized in the top right (C-terminal) side of the interdomain cleft, next to the tip of the blue triangular area. Anionic lipids may affect the access of the DAG acceptor to this donor site (see Discussion).

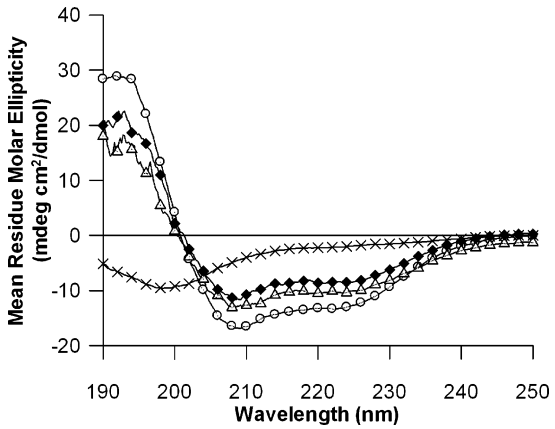

FIGURE 5: CD spectra for the alMGS peptide in different environments. One millimolar peptide in 100 mM DHPC micelles (○); DMPC/DHPC bicelles (q = 0.25) (◆); 30% acidic bicelles (q = 0.25, and [DMPG]/[DMPC] = 0.3) (△); and 100 mM phosphate buffer, pH 5.6 (×); all recorded at 37 °C.

Figure 1B. On the basis of these findings, the segment 65-SLKGFRLVLFVKRYVRKMRKLKL-87 (S65-L87) in alMGS (cf. Figure 3) was selected as a potential membrane-binding segment.

CD Analysis. Circular dichroism measurements of a synthetic S65-L87 peptide were performed in several different membrane-mimicking environments (H_2O, DHPC, zwitterionic bicelles, and acidic (anionic) bicelles) in order to determine the overall conformation (Figure 5). The CD spectra indicate an α-helix conformation in all solvents except water, with a mean molar ellipticity at 222 nm of −13307° cm²/dmol in DHPC solution, −8611 ° cm²/dmol in zwitterionic bicelle solution (q = 0.30), and −10492° cm²/dmol in 30% anionic bicelle solution (q = 0.30). This translates to an estimated α-helix content of 43% in the DHPC solution, 31% in a zwitterionic (i.e., PC) bicelle solution, and 36% in an anionic bicelle solution (i.e., with PG), respectively. A somewhat larger amount of helix is thus observed in DHPC micelles, which agrees with previous observations for peptides in different solvents (*33*). The absolute amount of helix is, however, difficult to determine quantitatively because differences in solubility and background may influence the spectra. Hence, a lipid environment seems to induce a helix conformation of the peptide, at both zwitterionic and anionic aggregate surface charges.

Binding Affinity of the Peptide to Lipid Bilayers. The affinity of S65-L87 to lipid bilayers was estimated by the surface plasmon resonance technique. Biacore L1 sensor chips were covered by liposomes according to established procedures. Because of the inherent anionic character of the chip surface, the extent of capture was reduced for anionic vesicles. Similar features have been observed by others (*43*).

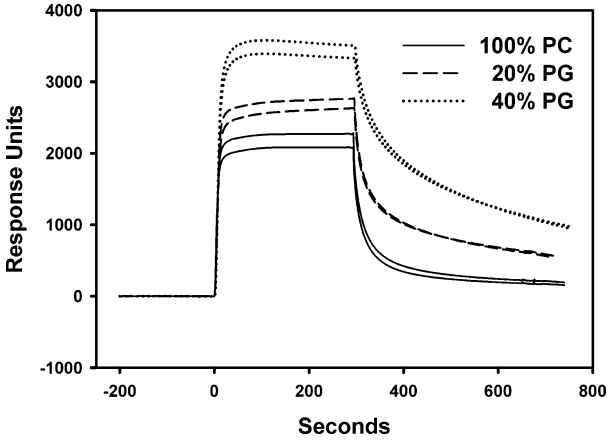

FIGURE 6: Lipid binding analyzed by SPR. Binding of alMGS peptide S65-L87 to liposome-coated Biacore L1 sensor chip surface. The peptide (5 μM) was injected at a flow rate of 5 μL/min over the different lipid surfaces, containing DOPC only, DOPC/DOPG 8:2, and DOPC/DOPG 6:4. Arrows denote the start and stop of peptide; duplicate experiments are shown.

Table 2: Structure Calculation Data for alMGS Peptide in 100 mM DHPC (24 Structures)

number of constraints	188
Dyana target function	0.07 ± 0.01 Å^2
maximum distance violation	0.11 ± 0.02 Å
backbone atom rmsd (Å)	
residues 3−23	2.42
residues 8−19	0.27
residue 8−16	0.20
Ramachandran plot regions (%)	
most favored regions	75.6
allowed regions	17.3
generously allowed regions	5.0
disallowed regions	2.1

This was compensated for by capturing DOPC vesicles (zwitterionic) in a subsequent second adsorption round, reaching similar final lipid amounts on the chip surfaces for all experiments and avoiding binding of the cationic peptide to the naked chip surface. The amount of peptide bound to the bilayer surfaces rose with increasing peptide concentrations (nano to micromolar range) for both DOPC (zwitterionic)- and DOPG-containing (anionic) bilayers. Figure 6 shows binding of S65-L87 at equilibrium conditions (plateu levels reached) with 5 μM peptide and buffer similar to that for the CD experiments. Binding was always fast, but the amounts of bound peptide during the association phase showed a complex dependence on injected concentrations, buffer salt strength, and mol % DOPG (data not shown). Especially at low peptide concentrations, the dissociation phase was dramatically different for the DOPC (fast) and DOPG (slow) bilayers. Potentially, this may depend on the competition between the hydrophobic and charge peptide properties for interaction with the lipid interface, which may also involve preferential orientations of the peptide close to the surface. At the higher peptide concentrations, bilayer affinity substantially increased by increasing the content of the anionic DOPG (as in Figure 6).

The CD analyses (Figure 5) showed the induction of a helix conformation, from a random, by both a PC and a PG lipid surface environment. Consequently, binding to these lipids (Figure 6) is likely to follow a two-state model, with potential formation of the helix at the bilayer surface/interface (*44*). Estimation of the dissociation constants (K_D) from the equilibrium states showed that K_D (M) for the peptide was in the range $10^{-7}-10^{-9}$ for 100% DOPC bilayers, $10^{-8}-10^{-12}$ for 20% DOPG (in DOPC), and 10^{-12} for 40% DOPG (in DOPC), depending on experimental conditions. This is analogous to the differential binding of PC and PG liposomes to the full size alMGS enzyme. The latter experiments also revealed similar affinities, with overall K_D values between 10^{-10} (M) for DOPC and $10^{-11}-10^{-12}$ for 20 and 40% DOPG (*12*). Hence, the S65-L87 peptide seems to have lipid bilayer-binding affinities fairly similar to that of the full-size alMGS enzyme.

Structure of S65-L87 Peptide According to Solution NMR. Two-dimensional TOCSY and NOESY spectra were recorded for the peptide in DHPC, neutral bicelles, and in (partly) negatively charged bicelles. Backbone assignments could be made for all but the two N-terminal residues in the peptide in DHPC (Ser65 and Leu66), and approximately 90% of the side chains were assigned. In the bicelle samples, assignments were made for H^N, H^α, and H^β protons. A structure was calculated for the alMGS peptide in DHPC, on the basis of 188 NOE-derived distances. No long-range NOEs were observed, but the sequential and medium-range NOEs as well as secondary H^α chemical shifts were consistent with a helical structure for at least part of the peptide, which made it possible to calculate the structure of the peptide in DHPC. The 24 best structures, with the lowest energies, were chosen to represent the final structure (Table 2, Figure 7). From analyses of hydrogen bond patterns and backbone torsion angles, it was found that the peptide adopts a helical structure between residues Leu71 and Met82. There is evidence that the helix extends even further toward the N-terminus, but because of overlap, not many NOE-derived distances typical for α-helix conformation were found for these residues.

From the ^{1}H NMR spectra in DHPC, neutral bicelle and acidic bicelle secondary chemical shifts for H^α (Figure 8a−c) and H^N (Figure 8d−e) were calculated according to ref *45*. In the DHPC environment, the H^α secondary shifts indicate a helical structure from at least Phe69 to Met82, a region that has extended to also include Arg83 and Lys84 in the neutral and acidic bicelle samples. Line broadening in the bicelle spectra made it virtually impossible to determine useful structural constraints to calculate a solution structure in those solvents, but because overall the H^α secondary shifts were fairly independent of changes in solvent, we conclude that the structure is similar in the three environments.

The differences between measured H^N chemical shifts and random coil values for the peptide were also calculated. These differences in the acidic and the neutral bicelle spectra are almost equal, and only slight differences between the bicelle results and those in DHPC are seen. In all three types of environments, the H^N secondary chemical shifts vary with a periodicity characteristic of an amphipathic α-helical structure. The results further suggest that the C-terminal is localized in a more hydrophilic surrounding (i.e., outside the membrane) than the rest of the peptide.

Positioning of S65-L87 in Neutral and Acidic Bicelles. A spin-labeled phospholipid was used to investigate the bicelle interaction of the peptide. The residues most affected by

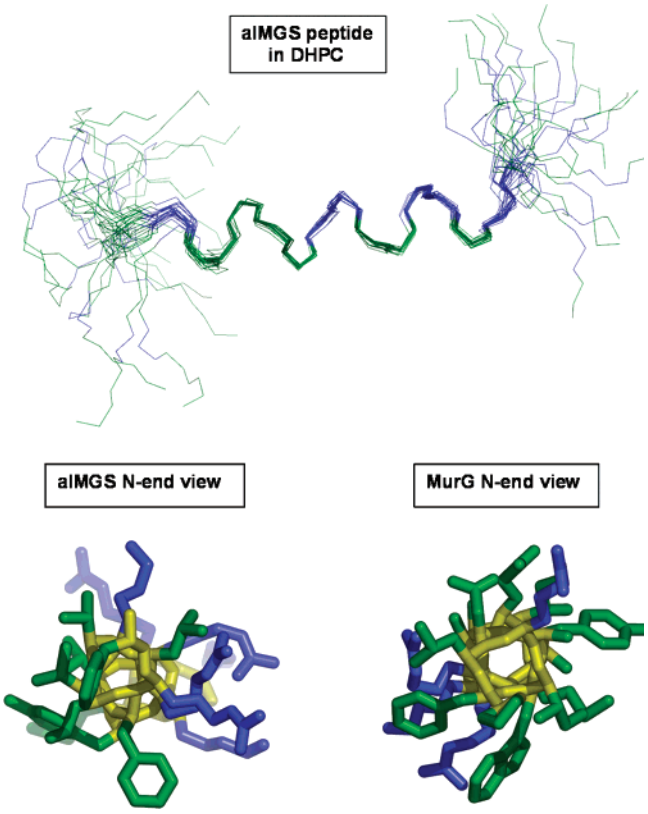

FIGURE 7: Solution structure of the alMGS peptide from NMR in 100 mM DHPC as represented by an ensemble of 24 structures. The overlay was done on backbone atoms in residues Lys67−Leu87 (N-terminal to the right). The bottom panels show end views (N-terminal outward) of the alMGS and the corresponding MurG peptide (cf. Figure 5). Positively charged residues are colored blue (cf. Figure 4).

the spin label were Gly68, Lys76, Arg80, and Leu85 (Figure 9). In zwitterionic bicelles, the signal corresponding to Met82 had disappeared. With the exception of the residues between Phe74 and Arg80, a fairly periodic behavior can be discerned, supporting the amphipathic α-helix character of the peptide residing in the interface between the acyl chain interior and the headgroup surface region. The residues in the C-terminal part are also less affected than the N-terminal ones, indicating that the charged C-terminus is situated outside of the bilayer. This agrees well with the secondary chemical shifts for the H^N protons. The results also indicate that the N-terminus of the peptide is inserted more deeply in the bilayer of the zwitterionic bicelles as compared to the partly charged (anionic) bicelles.

Influence on Lipid Packing as Monitored by DSC and ^{31}P NMR. Depending on the extent of bilayer lateral penetration by a peptide, the packing features of the lipid constituents will be differently affected. The ability of the S65-L87 peptide to modulate the lamellar to reversed hexagonal transition of hydrated DPoPE (zwitterionic) lipids was analyzed with differential scanning calorimetry. In addition to raising the bilayer to hexagonal phase transition temperature, introduction of a second component, the peptide in this case, causes loss of cooperativity of the transition resulting in broadening of the transition. An accurate bilayer to hexagonal transition temperature cannot be obtained at mole fractions much greater than 0.005 for this large peptide. With increasing mole fractions of peptide, stepwise from 0.00114 to 0.00453, the transition temperature rose as shown in Figure 10. This strongly indicates that the peptide intercalates in the interface, between the polar headgroups of DPoPE, and stabilizes the bilayer phase by promoting a more positive (less negative) curvature (*46*).

The morphology and phase equilibria of lipid aggregates can be assessed by ^{31}P NMR. Spectra were obtained from suspensions of DOPE/DOPG (7:3 mol/mol), analogous to the *in vivo* phospholipid composition of *E. coli* inner membranes. This mixture has a transition (two-phase region) from a lamellar (bilayer) to an isotropic (potentially cubic) phase between 45 and 70 °C (Figure 11, left column). At a lipid/peptide ratio of 30/1, that is, substantially more peptide than in the DSC experiments, this transition was suppressed and a bilayer organization maintained at all temperatures; cf. the absence of an isotropic peak in Figure 11, middle column. Here, the amounts of peptide plus charge and PG minus charge are fairly similar (PE zwitterionic charges not included). Hence, the nonbilayer-prone DOPE participates in a lamellar phase (with DOPG) at higher temperatures with peptide present, according to the chemical shift anisotropies. Likewise, the bilayer-prone DOPG participates in the isotropic phase (with DOPE) without peptide (Figure 11, left column). At a lipid/peptide ratio of 15/1 (Figure 11, right column), there is a substantial excess of peptide plus charges (10/peptide) over anionic DOPG in the mixture, and here, an isotropic phase was present in equilibrium with a lamellar one between 60 and 90 °C, although the isotropic component was a small fraction of the total powder pattern and was broader than that for the lipid alone. Potentially, the cluster of plus charges in the C-terminal region of S65-L87 may withdraw DOPG by complex formation to a lamellar phase in a portion of the sample and thereby allow the formation of an isotropic phase by the remaining DOPE. Hence, the peptide affects the packing of both zwitterionic and anionic lipids, and at low peptide amounts, this clearly supports an intercalation of the peptide in the bilayer interphase between the polar headgroups, promoting a more positive curvature strain.

The middle part of S65-L87 contains a (potential) CRAC cholesterol binding motif, L/V-(X)(1-5)-Y-(X)(1-5)-R/K, identified as a common element in proteins that have interactions with cholesterol (*47*). Certain peptides with this motif are found to sequester cholesterol into domains (*48*). However, analysis with DSC of various SOPG/cholesterol/peptide mixtures showed that the ability of the peptide to cause sequestration of cholesterol was very weak (data not shown). The high content of basic residues in this CRAC segment is not typical for such motifs, and this may relate to the inability of this peptide to interact with cholesterol. Still, the presence of a cholesterol-binding motif in a mycoplasma regulatory protein would potentially be biologically functional because these small bacteria are surface parasites on eukaryotes and incorporate cholesterol in their membranes, which affects alMGS activity *in vitro* as well as *in vivo*.

DISCUSSION

Features of Bilayer Interface-Binding Glycosyltransferases. From the combined multivariate and bioinformatic

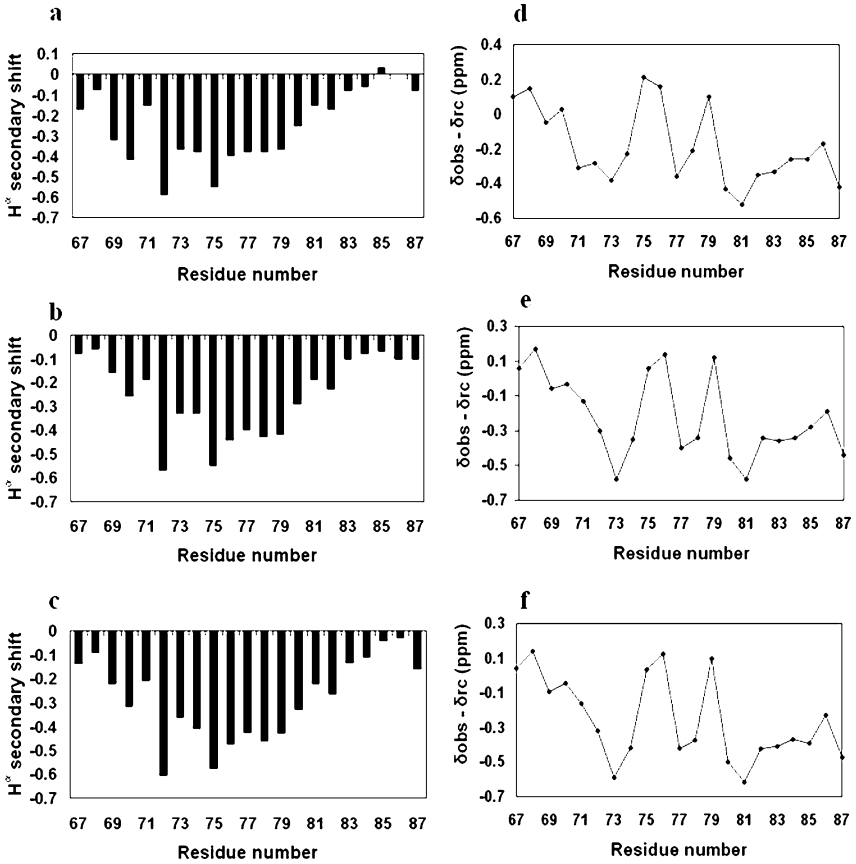

FIGURE 8: Secondary chemical shifts. Secondary chemical shifts for the alMGS peptide in (a) 100 mM DHPC; (b) DMPC/DHPC (q = 0.25) bicelles; and in (c) partly negatively charged bicelles ([DMPG]/[DMPC] = 0.1, and q = 0.25). Secondary H^N chemical shifts for the alMGS peptide in (d) 100 mM DHPC; (e) DMPC/DHPC (q = 0.25) bicelles; and in (f) partly negatively charged bicelles [DMPG]/[DMPC] = 0.1; and q = 0.3.

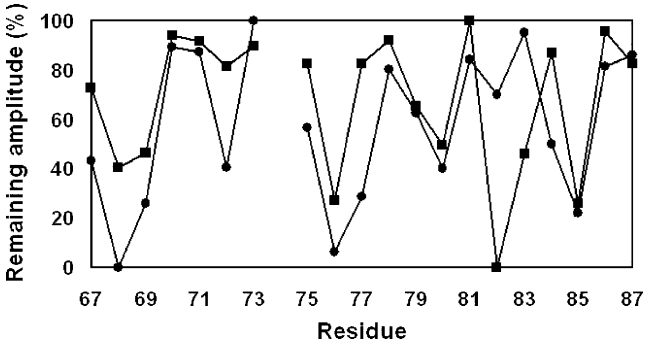

FIGURE 9: Intensity of H^N-H^α cross-peaks in TOCSY with spin label. One millimolar alMGS peptide in neutral DMPC/DHPC bicelles (●) and in 10% acidic bicelles, [DMPG]/[DMPC] = 0.1 (■), after the addition of 0.75 mM 1-palmityl-2-steroyl-(5-DOXYL)-*sn*-glycero-3-phosphocholine (t_{mix} = 30 ms).

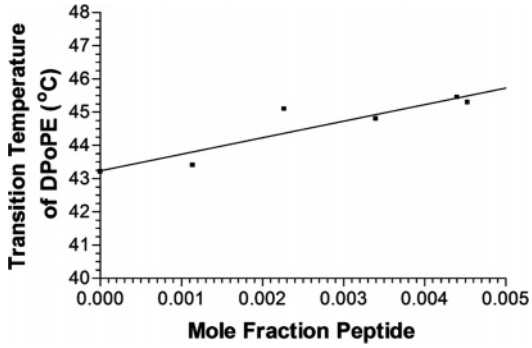

FIGURE 10: Dependence of the bilayer to hexagonal phase transition temperature. DPoPE was mixed with different mole fractions of the S65-L87 peptide. The positive linear regression of the line joining all of the points provides a measure of the promotion of positive curvature by the peptide.

sequence analyses plus several structural methods here, certain features for membrane-bound glycosyltransferases of the GT-B fold (lacking transmembrane segments) are evident.

(i) Amino Acid Sequence Properties. The most highly ranked factor according to the PLS grouping in Figure 1 is the high pI of the N-domains, followed by the pI of the full-size proteins. This is also clearly indicated from Table 1. It is well established that a high content of positively charged (cationic) amino acid residues promotes membrane surface binding of both soluble and amphipathic proteins and peptides by interactions with, especially, anionic phospholipids. Recently, from a support vector machine analysis, cationic protein surface charge was shown to be the major character of soluble C2 domains (with established structures) interacting with phospholipids at membrane interfaces (*49*). The latter study also revealed a higher surface proportion of aliphatic (V, L, I, and M) and aromatic aa's (especially W) and also C and K/R on the structures. In re-entrant regions between TM helices in integral membrane protein structures, small aa's, Trp, and Tyr and a certain fraction of hydrophobic aa's were recently recorded (*50*). The sequence-based multivariate method used here ranked volume and charge correlations between positions 1 and 9 (in the sliding window) as the third and fourth factor in terms of importance. These aa's were ones with a smaller side-chain volumes (such as G, V, I, A, L, and T) and frequently in loops,

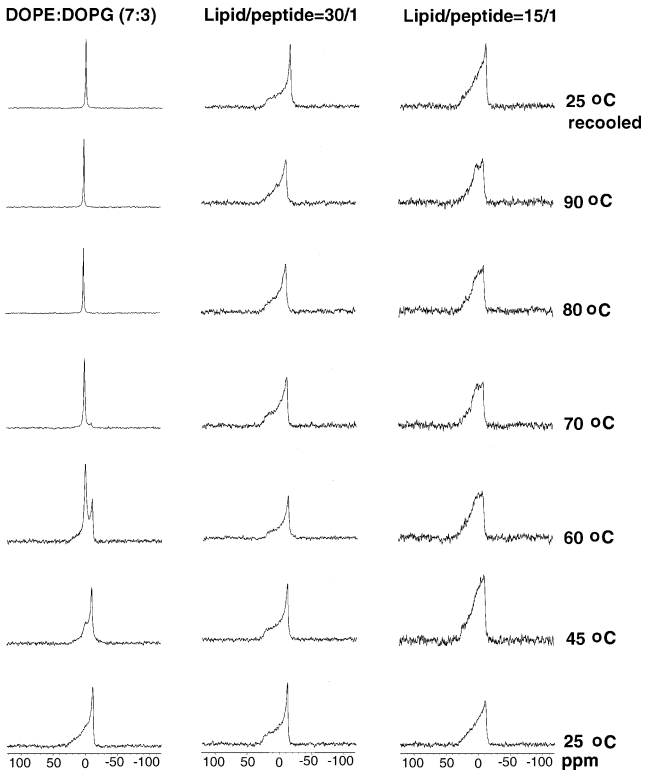

FIGURE 11: Effect of S65-L87 peptide on phospholipid packing. ^{31}P NMR as a function of temperature with DOPE/DOPG (7:3) ("membrane mimick") as a control (left column) and lipids with peptide (middle and right columns).

correlating in prevalence with, especially, K and R (in a helix or loop). Likewise, K and R correlated with K and R at position 9 and also often in loops. It may be anticipated that these loops can intercalate among the lipid headgroups such as the re-entrant segments of TM proteins.

It is noteworthy that tryptophan content was not a decisive factor for the multivariate separation of the membrane-associated GT group from the soluble one in Figure 1 (data not shown), as it was for the C2 structures and re-entrant segments (above). W is usually enriched in the so-called "aromatic girdle" at the membrane interface of transmembrane segments and is common in surface-associated helices and loops (*51*). Trp also has the largest ΔG value of all aa's for interface localization (*52*). MurG and alMGS, both localized to the right in the membrane PLS cluster (Figure 1) and with similar charge (high pI) properties (Table 1), may illustrate differences in association for these GTs. Both enzymes bind to membranes, but alMGS has only one Trp (W59) in the sequence, whereas MurG has eight (Figure 2). However, alMGS has 10 positive aa pairs (KK, KR, and RK, in addition to all single K and R) and all but one in the N-domain, whereas MurG only has one pair in total (Figure 2). Three of the Trp's in MurG (W116, W137, W291) are localized fairly close to the potential membrane-binding segment and one (W85) in the potential membrane-binding segment (Figure 4). These are also within the predicted interface-seeking segments (by MPEx; Figure 2). Likewise, the majority of the aa plus charge pair in the alMGS patch on the surface of the S65-L87 peptide region (cf. Figure 4). This may be a reflection of the different major lipids in the *A. laidlawii* and *E. coli* membranes being dominated by noncharged glucolipids and a zwitterionic phospholipid (PE), respectively. In addition, both species have a minority fraction of anionic phospholipids in their membranes. Alternatively, it reflects differences in how the lipid matrixes may influence or control the corresponding GT activities. The latter is supported by the K/R pair versus W content in two other *E. coli* GT-B structures with acceptor (lipid) substrates in the membrane: WaaC and WaaG (*53*, *54*). These two both have high pI values and 5/8 and 4/3 K/R pairs over W, respectively, that is, fairly different from the 1/8 relationship in MurG above. Analogous differences exist for more GTs in the set analyzed (Table 1), with the *Bacillus subtilis* and *Borrelia burgdorferi* lipid GTs in the low-Trp group with 7/0 and 10/2 of KR pairs/W. The latter cell is very rich in noncharged membrane glycolipids (data not shown).

Similarities with other proteins are also evident. A recent compilation of aa ligands binding directly to lipid headgroups in (mostly integral) membrane protein structures lists K, R, H, and Y/W as common ones (*55*). These are also found, including plus-charged doublets/triplets, in binding motifs of soluble proteins binding to the anionic phosphatidic acid and phosphatidylserine membrane lipids (*56*). In secreted (soluble) phospholipases A2, tryptophan at the binding surfaces promotes association with zwitterionic phospholipid interfaces, whereas K and R enhance binding and activity for anionic lipid membranes (*57*, *58*).

Hence, from the multivariate sequence property analyses of membrane surface-bound glycosyltransferases here (Table 1 and Figure 1), we conclude that the high content of positively charged aa's, that is, the high pI, is a key signature factor for this group of enzymes and is likely to attract and anchor the proteins to anionic phospholipids. Furthermore, the varying contents of K/R pairs and W are probably related to host membrane lipid composition and regulatory demands.

(*ii) Amphipathic Helices.* Variables describing the amphipathicity ("sidedness") of helices, that is, charge and hydrophobicity at position 1 versus position 3 in the window, ranked fifth and sixth in the multivariate analyses. Such helices were clearly identified from the MetaServer fold recognition and MOMENT sequence analyses (Figure 2) and coincided localization-wise in the predicted structure for alMGS with a suggested membrane-binding helix in the MurG structure, as illustrated in Figure 4. However, aa sequence conservation for these segments were lower than that for the rest of the proteins when comparing with many homologues (Figure 3). The N-terminal part of S65-L87 is similar to the amphipathic bilayer-binding helix motif of the conserved bacterial cell division protein MinD, which tolerates fairly large amino acid changes as long as amphipathicity is kept (*59*). The C-terminal plus-charge cluster of S65-L87 (KRYVRKMRK) is present in a number of other prokaryotic/eukaryotic proteins, including an archaeal glycosyltransferase (according to a BLAST analysis). The bee venom helical peptide melittin also has a similar C-terminal cluster (KRKR), and deleting these aa's one by one increased the hemolytic activity (*60*). Changing K76 and R77 to the negatively charged E in the alMGS enzyme stimulated enzyme activity *in vitro* at higher fractions of PG (data not shown). Together, this may indicate that the overall amphipathic properties of the helices are overriding the individual aa properties or that the sequence differences reflect different features in helix binding and orientation.

The NMR and CD analyses clearly support the predicted helical, amphipathic nature of the alMGS peptide formed at a bilayer interface. The helicity of the peptide was stronger in zwitterionic lipids than in anionic ones. The latter lipids may force a twist/orientation on the peptide because of its many positively charged residues. The peptide also revealed a slight tilt with respect to its orientation along the interface; the more hydrophobic N-terminal region was located deeper into the hydrophobic core than the highly charged C-terminal region, which seemed to reside just outside the bilayer. This was also indicated by comparing the MPEx and MOMENT analyses, where the latter method showed the amphipathic character proceeding downstream, outside the more N-terminal interface segment suggested by MPEx (Figure 2). Tilted peptides may destabilize bilayers (*61*), but the end view of the alMGS peptide strongly supports an interface localization due to its broad hydrophobic and charged sectors (Figure 7). The effect of the peptide on the phase equilibria ("packing properies") of zwitterionic as well as anionic bilayer systems (Figures 10 and 11) substantiates the interface localization indicated from the NMR structural analyses.

(*iii*) *Membrane Binding.* Proteins and peptides interacting with membrane surfaces can bind permanently or transiently to membranes. The latter is typical for phospholipases and signaling proteins binding to organelle identity lipid markers. The dissociation constant (K_D) for S65-L87 was low enough ($10^{-7}-10^{-9}$ M) even for zwitterionic PC bilayers to indicate an essentially permanent interface presence of the peptide; this was decreased further by anionic lipids, down to 10^{-12} (Figure 6). Formally, this refers to peptide in relation to binding sites in the chip-associated bilayers, and these lipid sites are not specified. As a comparison, K_D was in the range $10^{-5}-10^{-6}$ M for binding of the cationic (amphipathic) peptides magainin (antibacterial) and melittin (lytic) to PE/PG (7/3) bilayers by the SPR technique and L1 chips (*62*). Melittin has an oligo-KR cluster similar to S65-L87 (cf. above). Likewise, for five different phospholipases A_2, K_D was in the range $10^{-8}-10^{-10}$ M for binding to PC and PG bilayers (*63*).

Hence, the S65-L87 peptide segment has a bilayer affinity stronger than that of several membrane-seeking, soluble proteins/peptides, and this is enhanced by anionic phospholipids, approaching the values recorded for the binding of liposomes to the full-size alMGS enzyme (*12*). Furthermore, the calculated ΔG values from MPEx, for potential interface-associating segments of alMGS (in Figure 2), are of just slightly smaller magnitude than for several interface-anchoring helices in monotopic integral membrane proteins such as prostaglandin synthase. For the corresponding segments in the consecutive alDGS enzyme, ΔG values were even closer to the monotopic proteins (data not shown).

Evolutionary and Functional Aspects. The membrane-binding features established here for the S65-L87 peptide of alMGS seem, by analogy to aa properties, to be present in many membrane surface-associated GTs of similar structure (cf. Figures 3 and 4). Interestingly, another key lipid enzyme, CTP, phosphocholine cytidylyltransferase has also been found to contain an amphipathic helical segment that is responsible for the enzyme activity being regulated by negative charge and negative curvature strain in the bilayer (*64*, *65*). The localization of such segments in the GT structures clearly indicates that the bilayer-binding characteristics have been evolutionarily introduced by aa modifications in/close to what is the binding region for acceptor substrates in soluble glycosyltransferases such as the template GtfB in Figure 2. In GtfB, −A and −D enzyme structures, a more or less deep acceptor substrate "bowl" is flanked by two helices (*18*−*20*) that are the structural analogues to the two amphipathic ones in alMGS (Figure 2). Likewise, the proposed membrane-binding helix of MurG has a similar location (Figure 4).

Surrounding the potential lipid acceptor substrate sites may be of functional significance, in addition to membrane binding. This is probably different for the eukaryotic GT-B fold lipid GT enzymes frequently containing one transmembrane segment, where the latter seem to be an attached anchor and organelle target segment (e.g., for ceramide-β-galactosyltransferase (UniProt code CGT_HUMAN)). However, amphipathic interface helices can also be inserted in an otherwise soluble enzyme for membrane anchoring, as for the carnitine palmitoyltransferase 2 structure (*66*). Likewise, the hydroxysteroid dehydrogenase (of Rossmann fold) has two unique membrane-associating helices, not present in the many soluble homologues, with membrane-anchoring typical for monotopic integral membrane proteins (*67*). Several soluble proteins contain cationic, amphipathic segments that act as lids over substrate pockets and that can also be engaged in membrane binding and sensing, as in the lipases from *Thermomyces lanuginosa* and *Candida rugosa*, the OSBP-related proteins, glycolipid transfer proteins, and certain StAR proteins (data not shown). In several of these segments, and in the anchoring interfaces of A2 phospholipases and helices in monotopic proteins, sequence variations between homologues are observed, in a manner similar to that for the S65-L87 helix segment from alMGS here (Figure 3). This may be explained as adaptations to or potential control by the local lipid environments in their target membranes (*58*, *68*) for the latter proteins.

Several monotopic membrane proteins have a substrate channel in between the anchoring interface-oriented helices, where the latter have to rotate or move to let substrate up into the active site (*69*). The localization of the two amphipathic segments in alMGS enclose the potential acceptor substrate (diacylglycerol) site (Figure 4), and an association of diacylglycerol with the anionic PG in lipid bilayers has been shown (*13*). PG and a nonbilayer-prone additive also affect the positioning of W59, just preceding S65-L87 (*12*). Could PG affect the orientation of the S65-L87 helix and bring in the acceptor diacylglycerol? Given the localization and flanking loop sequences, and strong charge and amphipathic properties, a displacement coupled to sensing and activity is potentially possible.

ACKNOWLEDGMENT

We thank Drs. Anders Öhman and Amelie Kelly for valuable discussions and Mrs. Preeti Vyas for performing the site-specific mutations of the alMGS enzyme.

REFERENCES

1. Morein, S., Andersson, A., Rilfors, L., and Lindblom, G. (1996) Wild-type *Escherichia coli* cells regulate the membrane lipid composition in a "window" between gel and non-lamellar structures, *J. Biol. Chem. 271*, 6801−6809.

2. Magnuson, K., Jackowski, S., Rock, C. O., and Cronan, J. E. Jr. (1993) Regulation of fatty acid biosynthesis in *Escherichia coli*, *Microbiol. Rev. 57*, 522−542.
3. Dahlqvist, A., Nordstrom, S., Karlsson, O. P., Mannock, D. A., McElhaney, R. N., and Wieslander, A. (1995) Efficient modulation of glucolipid enzyme activities in membranes of *Acholeplasma laidlawii* by the type of lipids in the bilayer matrix, *Biochemistry 34*, 13381−13389.
4. Karlsson, O. P., Dahlqvist, A., Vikstrom, S., and Wieslander, A. (1997) Lipid dependence and basic kinetics of the purified 1,2-diacylglycerol 3-glucosyltransferase from membranes of *Acholeplasma laidlawii*, *J. Biol. Chem. 272*, 929−936.
5. Vikstrom, S., Li, L., Karlsson, O. P., and Wieslander, A. (1999) Key role of the diglucosyldiacylglycerol synthase for the nonbilayer-bilayer lipid balance of *Acholeplasma laidlawii* membranes, *Biochemistry 38*, 5511−5520.
6. Lindblom, G., Brentel, I., Sjolund, M., Wikander, G., and Wieslander, A. (1986) Phase equilibria of membrane lipids from *Acholeplasma laidlawii*: importance of a single lipid forming nonlamellar phases, *Biochemistry 25*, 7502−7510.
7. Andersson, A. S., Rilfors, L., Bergqvist, M., Persson, S., and Lindblom, G. (1996) New aspects on membrane lipid regulation in *Acholeplasma laidlawii* A and phase equilibria of monoacyldiglucosyldiacylglycerol, *Biochemistry 35*, 11119−11130.
8. Wieslander, A., Rilfors, L., and Lindblom, G. (1986) Metabolic changes of membrane lipid composition in *Acholeplasma laidlawii* by hydrocarbons, alcohols, and detergents: arguments for effects on lipid packing, *Biochemistry 25*, 7511−7517.
9. Wikstrom, M., Xie, J., Bogdanov, M., Mileykovskaya, E., Heacock, P., Wieslander, A., and Dowhan, W. (2004) Monoglucosyldiacylglycerol, a foreign lipid, can substitute for phosphatidylethanolamine in essential membrane-associated functions in *Escherichia coli*, *J. Biol. Chem. 279*, 10484−10493.
10. Edman, M., Berg, S., Storm, P., Wikstrom, M., Vikstrom, S., Ohman, A., and Wieslander, A. (2003) Structural features of glycosyltransferases synthesizing major bilayer and nonbilayer-prone membrane lipids in *Acholeplasma laidlawii* and *Streptococcus pneumoniae*, *J. Biol. Chem. 278*, 8420−8428.
11. Davies, G. J., Gloster, T. M., and Henrissat, B. (2005) Recent structural insights into the expanding world of carbohydrate-active enzymes, *Curr. Opin. Struct. Biol. 15*, 637−645.
12. Li, L., Storm, P., Karlsson, O. P., Berg, S., and Wieslander, A. (2003) Irreversible binding and activity control of the 1,2-diacylglycerol 3-glucosyltransferase from *Acholeplasma laidlawii* at an anionic lipid bilayer surface, *Biochemistry 42*, 9677−9686.
13. Storm, P., Li, L., Kinnunen, P., and Wieslander, A. (2003) Lateral organization in *Acholeplasma laidlawii* lipid bilayer models containing endogenous pyrene probes, *Eur. J. Biochem. 270*, 1699−16709.
14. Karlsson, O. P., Dahlqvist, A., and Wieslander, A. (1994) Activation of the membrane glucolipid synthesis in *Acholeplasma laidlawii* by phosphatidylglycerol and other anionic lipids, *J. Biol. Chem. 269*, 23484−23490.
15. Hurley, J. H. (2006) Membrane binding domains, *Biochim. Biophys. Acta 1761*, 805−811.
16. Mulgrew-Nesbitt, A., Diraviyam, K., Wang, J., Singh, S., Murray, P., Li, Z., Rogers, L., Mirkovic, N., and Murray, D. (2006) The role of electrostatics in protein-membrane interactions, *Biochim. Biophys. Acta 1761*, 812−826.
17. Ha, S., Walker, D., Shi, Y., and Walker, S. (2000) The 1.9 Å crystal structure of *Escherichia coli* MurG, a membrane-associated glycosyltransferase involved in peptidoglycan biosynthesis, *Protein Sci. 9*, 1045−1052.
18. Mulichak, A. M., Losey, H. C., Lu, W., Wawrzak, Z., Walsh, C. T., and Garavito, R. M. (2003) Structure of the TDP-epivancosaminyltransferase GtfA from the chloroeremomycin biosynthetic pathway, *Proc. Natl. Acad. Sci. U.S.A. 100*, 9238−9243.
19. Mulichak, A. M., Losey, H. C., Walsh, C. T., and Garavito, R. M. (2001) Structure of the UDP-glucosyltransferase GtfB that modifies the heptapeptide aglycone in the biosynthesis of vancomycin group antibiotics, *Structure 9*, 547−557.
20. Mulichak, A. M., Lu, W., Losey, H. C., Walsh, C. T., and Garavito, R. M. (2004) Crystal structure of vancosaminyltransferase GtfD from the vancomycin biosynthetic pathway: interactions with acceptor and nucleotide ligands, *Biochemistry 43*, 5170−5180.
21. Berg, S., Edman, M., Li, L., Wikstrom, M., and Wieslander, A. (2001) Sequence properties of the 1,2-diacylglycerol 3-glucosyltransferase from *Acholeplasma laidlawii* membranes. Recognition of a large group of lipid glycosyltransferases in eubacteria and archaea, *J. Biol. Chem. 276*, 22056−22063.
22. Wimley, W. C., and White, S. H. (1996) Experimentally determined hydrophobicity scale for proteins at membrane interfaces, *Nat. Struct. Biol. 3*, 842−848.
23. Hellberg, S., Sjöström, M., Skagerberg, B., and Wold, S. (1987) Peptide quantitative structure-activity relationships, a multivariate approach, *J. Med. Chem. 30*, 1126−1135.
24. Rosen, M. L., Edman, M., Sjostrom, M., and Wieslander, A. (2004) Recognition of fold and sugar linkage for glycosyltransferases by multivariate sequence analysis, *J. Biol. Chem. 279*, 38683−38692.
25. Greenfield, N., and Fasman, G. D. (1969) Computed circular dichroism spectra for the evaluation of protein conformation, *Biochemistry 8*, 4108−4116.
26. MacDonald, R. C., MacDonald, R. I., Menco, B. P., Takeshita, K., Subbarao, N. K., and Hu, L. R. (1991) Small-volume extrusion apparatus for preparation of large, unilamellar vesicles, *Biochim. Biophys. Acta 1061*, 297−303.
27. Jeener, J., Meier, B., Bachman, P., and Ernst, R. R. (1979) Investigation of exchange process by two-dimensional NMR spectroscopy, *J. Chem. Phys. 71* 4546−4563.
28. Braunschweiler, L., and Ernst, R. R. (1983) Coherence transfer by isotropic mixing: application to proton correlation spectroscopy, *J. Magn. Reson. 53*, 521−528.
29. Piotto, M., Saudek, V., and Sklenar, V. (1992) Gradient-tailored excitation for single-quantum NMR spectroscopy of aqueous solutions, *J. Biomol. NMR 2*, 661−665.
30. Guntert, P., Mumenthaler, C., and Wuthrich, K. (1997) Torsion angle dynamics for NMR structure calculation with the new program DYANA, *J. Mol. Biol. 273*, 283−298.
31. Laskowski, R. A., MacArthur, M. W., Moss, D. S., and Thornton, J. M. (1993) PROCHECK: a program to check the stereochemical quality of protein structures, *J. Appl. Crystallogr. 26*, 283−291.
32. Damberg, P., Jarvet, J., and Graslund, A. (2001) Micellar systems as solvents in peptide and protein structure determination, *Methods Enzymol. 339*, 271−285.
33. Biverstahl, H., Andersson, A., Graslund, A., and Maler, L. (2004) NMR solution structure and membrane interaction of the N-terminal sequence (1−30) of the bovine prion protein, *Biochemistry 43*, 14940−14947.
34. Lindberg, M., Biverstahl, H., Graslund, A., and Maler, L. (2003) Structure and positioning comparison of two variants of penetratin in two different membrane mimicking systems by NMR, *Eur. J. Biochem. 270*, 3055−3063.
35. Abrams, F. S., and London, E. (1993) Extension of the parallax analysis of membrane penetration depth to the polar region of model membranes: use of fluorescence quenching by a spin-label attached to the phospholipid polar headgroup, *Biochemistry 32*, 10826−10831.
36. Chattopadhyay, A., and London, E. (1987) Parallax method for direct measurement of membrane penetration depth utilizing fluorescence quenching by spin-labeled phospholipids, *Biochemistry 26*, 39−45.
37. Imberty, A., Wimmerova, M., Koca, J., and Breton, C. (2006) Molecular modeling of glycosyltransferases, *Methods Mol. Biol. 347*, 145−156.
38. Engel, D. E., and DeGrado, W. F. (2004) Amino acid propensities are position-dependent throughout the length of alpha-helices, *J. Mol. Biol. 337*, 1195−1205.
39. Leonov, H., and Arkin, I. T. (2005) A periodicity analysis of transmembrane helices, *Bioinformatics 21*, 2604−2610.
40. Kim, S., Jeon, T. J., Oberai, A., Yang, D., Schmidt, J. J., and Bowie, J. U. (2005) Transmembrane glycine zippers: physiological and pathological roles in membrane proteins, *Proc. Natl. Acad. Sci. U.S.A. 102*, 14278−14283.
41. Ridder, A., Skupjen, P., Unterreitmeier, S., and Langosch, D. (2005) Tryptophan supports interaction of transmembrane helices, *J. Mol. Biol. 354*, 894−902.
42. Eisenberg, D., Schwarz, E., Komaromy, M., and Wall, R. (1984) Analysis of membrane and surface protein sequences with the hydrophobic moment plot, *J. Mol. Biol. 179*, 125−142.
43. Besenicar, M., Macek, P., Lakey, J. H., and Anderluh, G. (2006) Surface plasmon resonance in protein-membrane interactions, *Chem. Phys. Lipids 141*, 169−178.
44. Mozsolits, H., and Aguilar, M. I. (2002) Surface plasmon resonance spectroscopy: an emerging tool for the study of peptide-membrane interactions, *Biopolymers 66*, 3−18.
45. Wishart, D. S., and Sykes, B. D. (1994) Chemical shifts as a tool for structure determination, *Methods Enzymol. 239*, 363−392.

46. Epand, R. F., Lehrer, R. I., Waring, A., Wang, W., Maget-Dana, R., Lelievre, D., and Epand, R. M. (2003) Direct comparison of membrane interactions of model peptides composed of only Leu and Lys residues, *Biopolymers 71*, 2−16.
47. Li, H., and Papadopoulos, V. (1998) Peripheral-type benzodiazepine receptor function in cholesterol transport. Identification of a putative cholesterol recognition/interaction amino acid sequence and consensus pattern, *Endocrinology 139*, 4991−4997.
48. Epand, R. M. (2006) Cholesterol and the interaction of proteins with membrane domains, *Prog. Lipid Res. 45*, 279−294.
49. Bhardwaj, N., Stahelin, R. V., Langlois, R. E., Cho, W., and Lu, H. (2006) Structural bioinformatics prediction of membrane-binding proteins, *J. Mol. Biol. 359*, 486−495.
50. Viklund, H., Granseth, E., and Elofsson, A. (2006) Structural classification and prediction of reentrant regions in alpha-helical transmembrane proteins: application to complete genomes, *J. Mol. Biol. 361*, 591−603.
51. Liu, W., and Caffrey, M. (2006) Interactions of tryptophan, tryptophan peptides, and tryptophan alkyl esters at curved membrane interfaces, *Biochemistry 45*, 11713−11726.
52. Wimley, W. C., Creamer, T. P., and White, S. H. (1996) Solvation energies of amino acid side chains and backbone in a family of host-guest pentapeptides, *Biochemistry 35*, 5109−5124.
53. Grizot, S., Salem, M., Vongsouthi, V., Durand, L., Moreau, F., Dohi, H., Vincent, S., Escaich, S., and Ducruix, A. (2006) Structure of the *Escherichia coli* heptosyltransferase WaaC: binary complexes with ADP and ADP-2-deoxy-2-fluoro heptose, *J. Mol. Biol. 363*, 383−394.
54. Martinez-Fleites, C., Proctor, M., Roberts, S., Bolam, D. N., Gilbert, H. J., and Davies, G. J. (2006) Insights into the synthesis of lipopolysaccharide and antibiotics through the structures of two retaining glycosyltransferases from family GT4, *Chem. Biol. 13*, 1143−1152.
55. Palsdottir, H., and Hunte, C. (2004) Lipids in membrane protein structures, *Biochim. Biophys. Acta 1666*, 2−18.
56. Stace, C. L., and Ktistakis, N. T. (2006) Phosphatidic acid- and phosphatidylserine-binding proteins, *Biochim. Biophys. Acta 1761*, 913−926.
57. Gelb, M. H., Cho, W., and Wilton, D. C. (1999) Interfacial binding of secreted phospholipases A(2): more than electrostatics and a major role for tryptophan, *Curr. Opin. Struct. Biol. 9*, 428−432.
58. Winget, J. M., Pan, Y. H., and Bahnson, B. J. (2006) The interfacial binding surface of phospholipase A2s, *Biochim. Biophys. Acta 1761*, 1260−1269.
59. Szeto, T. H., Rowland, S. L., Rothfield, L. I., and King, G. F. (2002) Membrane localization of MinD is mediated by a C-terminal motif that is conserved across eubacteria, archaea, and chloroplasts, *Proc. Natl. Acad. Sci. U.S.A. 99*, 15693−15698.
60. Blondelle, S. E., and Houghten, R. A. (1991) Hemolytic and antimicrobial activities of the twenty-four individual omission analogues of melittin, *Biochemistry 30*, 4671−4678.
61. Brasseur, R. (2000) Tilted peptides: a motif for membrane destabilization (hypothesis), *Mol. Membr. Biol. 17*, 31−40.
62. Papo, N., and Shai, Y. (2003) Exploring peptide membrane interaction using surface plasmon resonance: differentiation between pore formation versus membrane disruption by lytic peptides, *Biochemistry 42*, 458−466.
63. Stahelin, R. V., and Cho, W. (2001) Differential roles of ionic, aliphatic, and aromatic residues in membrane-protein interactions: a surface plasmon resonance study on phospholipases A2, *Biochemistry 40*, 4672−4678.
64. Davies, S. M., Epand, R. M., Kraayenhof, R., and Cornell, R. B. (2001) Regulation of CTP: phosphocholine cytidylyltransferase activity by the physical properties of lipid membranes: an important role for stored curvature strain energy, *Biochemistry 40*, 10522−10531.
65. Drobnies, A. E., Davies, S. M., Kraayenhof, R., Epand, R. F., Epand, R. M., and Cornell, R. B. (2002) CTP:phosphocholine cytidylyltransferase and protein kinase C recognize different physical features of membranes: differential responses to an oxidized phosphatidylcholine, *Biochim. Biophys. Acta 1564*, 82−90.
66. Rufer, A. C., Thoma, R., Benz, J., Stihle, M., Gsell, B., De Roo, E., Banner, D. W., Mueller, F., Chomienne, O., and Hennig, M. (2006) The crystal structure of carnitine palmitoyltransferase 2 and implications for diabetes treatment, *Structure 14*, 713−723.
67. Ogg, D., Elleby, B., Norstrom, C., Stefansson, K., Abrahmsen, L., Oppermann, U., and Svensson, S. (2005) The crystal structure of guinea pig 11beta-hydroxysteroid dehydrogenase type 1 provides a model for enzyme-lipid bilayer interactions, *J. Biol. Chem. 280*, 3789−3794.
68. MirAfzali, Z., Leipprandt, J. R., McCracken, J. L., and DeWitt, D. L. (2006) Topography of the prostaglandin endoperoxide H2 synthase-2 in membranes, *J. Biol. Chem. 281*, 28354−28364.
69. Garavito, R. M., and Mulichak, A. M. (2003) The structure of mammalian cyclooxygenases, *Annu. Rev. Biophys. Biomol. Struct. 32*, 183−206.

BI700042X